Nonlinearly coupled localized plasmon resonances: Resonant second-harmonic generation

Pavel Ginzburg,[1,*] Alexey Krasavin,[1] Yannick Sonnefraud,[2] Antony Murphy,[3] Robert J. Pollard,[3] Stefan A. Maier,[2] and Anatoly V. Zayats[1]

[1]*Department of Physics, King's College London, Strand, London WC2R 2LS, United Kingdom*
[2]*Imperial College London, Blackett Laboratory, Experimental Solid State Group, London SW7 2AZ, United Kingdom*
[3]*Centre for Nanostructured Media, The Queen's University of Belfast, Belfast, BT7 1NN, United Kingdom*

(Received 21 May 2012; published 13 August 2012)

The efficient resonant nonlinear coupling between localized surface plasmon modes is demonstrated in a simple and intuitive way using boundary integral formulation and utilizing second-order optical nonlinearity. The nonlinearity is derived from the hydrodynamic description of electron plasma and originates from the presence of material interfaces in the case of small metal particles. The coupling between fundamental and second-harmonic modes is shown to be symmetry selective and proportional to the spatial overlap between polarization dipole density of the second-harmonic mode and the square of the polarization charge density of the fundamental mode. Particles with high geometrical symmetry will convert a far-field illumination into dark nonradiating second-harmonic modes, such as quadrupoles. Effective second-harmonic susceptibilities are proportional to the surface-to-volume ratio of a particle, emphasizing the nanoscale enhancement of the effect.

DOI: 10.1103/PhysRevB.86.085422 PACS number(s): 73.20.Mf, 42.65.Ky, 78.67.Bf

I. INTRODUCTION

Nonlinear optics has triggered the evolution of modern optics, yielding discoveries of important phenomena, deep understandings of fundamental optical effects and, moreover, serving as a source for a large variety of applications. Nonlinear optical interactions are relatively weak but can be significantly enhanced using various approaches. Generally, nonlinear optical phenomena are proportional to higher orders of the driving field, motivating the quest for local electromagnetic field enhancement for which various nanostructures have been proven to be beneficial. In particular, noble metals with negative permittivity at optical and infrared wavelengths can support the so-called surface plasmon modes with the deep-subwavelength localization of the electromagnetic energy, overcoming the conventional diffraction limit and leading to the field enhancement effects.[1] Plasmonic nanostructures are perfect candidates for the realization of various concepts for the enhancement of nonlinear effects. Surface-enhanced Raman scattering (SERS) is one of the most famous examples of plasmonic-enhanced processes: a rough noble metal surface was shown to enhance the magnitude of the scattering by 14 orders of magnitude compared to the conventional process.[2] The advantage of doubly resonant plasmonic structures was demonstrated for SERS where a pair of particles provides the resonant enhancement for both the pump and Stokes frequencies.[3] The grooves etched in a metal surface and organized into a grating geometry have been shown to enhance the four-wave mixing (FWM) efficiency by two orders of magnitude.[4] Four orders of magnitude improvement of FWM was demonstrated with a plasmonic dimer configuration.[5] Optical nonlinearities assisted by plasmonic nanostructures have recently been proposed for various applications in active photonic components,[6] sensing,[7] and signal processing.[8]

Second-harmonic generation (SHG) is the most basic nonlinear process in which two photons combine to create a photon at double frequency. There are many literature reports on the study of various SHG-based plasmonic devices. For instance, core-shell nanocavities have been shown to enhance the nonlinear SHG conversion in a nonlinear core by two to three orders of magnitude.[9] Nanorings of GaAs incorporated in a gold film have been shown to enhance the SHG in the wavelength range corresponding to the enhanced transmission of the film.[10] Dark plasmonic modes (weakly coupled to far-field radiation) may be excited via second-harmonic generation.[11] SHG from small metal clusters and rough surfaces was investigated in Ref. 12, although the multiple resonant structure was ignored. In the previous studies, nonlinear interactions were considered to originate from either nonlinear dielectric materials and then be enhanced by the metal structures or bulk and surface metal nonlinearities, which are not always straightforward to distinguish.[13]

Furthermore, nanoscale nonlinear processes are essentially different from conventional nonlinear phenomena.[14] One of the fundamental requirements of the "propagating-wave" nonlinear optics is the fulfillment of phase-matching conditions: fundamental and second-harmonic waves have to propagate in phase in order to create constructive interferences and, thus, considerably increase the efficiency of the conversion process.[15] The possibility of fabricating small photonic cavities initiated the studies of cavity nonlinear optics where the classical phase-matching conditions are replaced by a spatial overlap of localized modes at fundamental and second harmonic frequencies in order to obtain an enhanced conversion efficiency.[16] Hence, investigations of nontrivial conditions for optimized nonlinear interactions in subwavelength plasmonic objects are of potential fundamental and applicative interest.

In this paper we develop the theoretical description of nonlinear interactions, in particular, SHG, in the nanoplasmonic environment taking into account intrinsic free-electron nonlinearity of metals. The role of the boundaries of nanostructures has been elucidated to play the key role in nonlinear

interactions. We have investigated the dynamics of nonlinearly coupled plasmonic modes in metal nanoparticles. The source of nonlinearity is the metal itself while the surrounding environment is assumed to be linear. We show that the most significant contribution to SHG originates from abrupt boundaries, while other bulk nonlinearity mechanisms are less important in the nanoplasmonic deep-subwavelength regime. The overlap integral ("cavity phase-matching condition")[16] is replaced by a boundary integration which provide a quantitative measure of the matching of the surface charge density (at fundamental wavelength) with the induced surface dipole density (at second-harmonic wavelength) to produce localized surface plasmon phase-matching condition, as will be further explained below. The distinctive result of our derivation is that the SHG efficiency is proportional to the ratio of surface area to volume, emphasizing the significant benefit of nanostructuring. Previously, size-dependent effects and polarization selection rules for SHG were studied for Rayleigh spheres made of centrosymmetric material.[17] Note also that nonlocal effects due to the strong electron confinement in plasmonic nanoparticles may lead to other nontrivial size-dependent effects.[18]

II. THEORETICAL FORMULATION

Hydrodynamic equations provide satisfactory description of electrons' dynamics in the conduction band of noble metals, such as silver and gold. In fact, hydrodynamic treatment was first used by Ritchie in his seminal work,[19] where he predicted the existence of surface plasmons. Traditionally, material susceptibilities, linear as well as nonlinear, are derived with the help of averaged quantities—electron density ($n = n_0 + n_1 e^{-i\omega t} + n_2 e^{-2i\omega t} + \cdots$) and average velocity ($v = v_1 e^{-i\omega t} + v_2 e^{-2i\omega t} + \cdots$). The basic result for linear response is the well-known Drude model, which fits experimental data considerably well away from the plasma frequency and interband transitions. Additional higher-order corrections and introduction of additional terms, such as quantum pressure of electron gas and viscosity, may lead to spatial dispersion contributions and temperature dependence of the appropriate optical constants (Ref. 20 and references therein and citing articles). Introduction of the conservative ponderomotive potentials may lead to third-order plasmalike nonlinearities of electron gas.[21] Careful inclusion of losses and interband transitions in the frame of the hydrodynamic model provides more detailed, but complex formulation.[22] However, the basic result of the Sommerfeld free-electron model extension for nonlinear polarizability $\overrightarrow{P}^{(2)}(\omega,\omega)$ is based on the derivations of Bloembergen *et al.*,[23] which is the core of other advanced models.

Expanding the electromagnetic fields in terms of basic and higher harmonics $\overrightarrow{E} = \overrightarrow{E_1}e^{-i\omega t} + \overrightarrow{E_2}e^{-2i\omega t} + \cdots$, $\overrightarrow{H} = \overrightarrow{H_1}e^{-i\omega t} + \overrightarrow{H_2}e^{-2i\omega t} + \cdots$ and substituting them into hydrodynamic equations $\frac{\partial v}{\partial t} + v\cdot\nabla v = -\frac{e}{m}(\overrightarrow{E} + \overrightarrow{v}\times\overrightarrow{H})$, $\nabla\cdot\overrightarrow{E} = -\frac{1}{\varepsilon}e(n-n_0)$, $\frac{\partial n}{\partial t} = -\nabla\cdot(n\overrightarrow{v})$, and $\overrightarrow{J} = -en\overrightarrow{v}$, where $\overrightarrow{J}$ is the current density, related to the polarization, the following expression for nonlinear polarizability may be obtained:[23]

$$\overrightarrow{P}^{(2)}(\omega,\omega) = -\left(\frac{\omega_p}{2\omega}\right)^2 \varepsilon_b \overrightarrow{E_2} + i\frac{e\varepsilon_b\omega_p^2}{4m\omega^3}\overrightarrow{E_1}\times\overrightarrow{H_1} + \frac{e\varepsilon_b\omega_p^2}{4m\omega^4}(\overrightarrow{E_1}\cdot\vec{\nabla})\overrightarrow{E_1} + \frac{e\varepsilon_b}{2m\omega^2}(\nabla\cdot\overrightarrow{E_1})\overrightarrow{E_1}, \quad (1)$$

where $\omega_p^2 = \frac{n_0 e^2}{m\varepsilon_b}$ is the electron plasma frequency, ω is the angular frequency of the field, n_0 is the concentration of the unperturbed electrons, m is the electron effective mass, and ε_b is the background permittivity. Taking the divergence of Eq. (1), we obtain the nonlinear polarization charge density, acting as the source for second harmonic field. Neglecting higher-order spatial derivatives of the fields within a particle and taking into account that the rotor of the electrical field vanishes under the quasistatic approximation, the second-order nonlinear polarization charge density can be represented as follows:

$$\rho_{NL}^{(2\omega)} = -\frac{e\varepsilon_b}{2m\omega^2}\left(\frac{\omega_p^2}{2\omega^2}+1\right)(\nabla\cdot\overrightarrow{E_1})^2. \quad (2)$$

Note that the divergence of electrical field is the only nonvanishing term on the boundaries, it corresponds to the surface charge density. This nonlinear charge serves as the source of the second-harmonic field.

As the next step, we derive the set of coupled-mode equations, representing the electromagnetic fields via the eign-modes of plasmonic resonances. We start from the nonlinear wave equation (neglecting material dispersion around the operation frequency) $\nabla\times\nabla\times\overrightarrow{E} = -\mu_0\varepsilon(\vec{r})\partial_{tt}\overrightarrow{E} - \mu_0\partial_{tt}\overrightarrow{P}_{NL}$, where $\varepsilon(\vec{r})$ is the spatial-dependent permittivity, $\overrightarrow{P}_{NL}$ is nonlinear polarizability, and ∂_{tt} is the second-order time derivative. We expand the electromagnetic fields obeying Maxwell's equations in a virtual cavity using following cavity modes:

$$\overrightarrow{E}_k = A_k(t)e^{-i\omega_k t}e^{-\gamma_k(\omega_k)t}\overrightarrow{F}_k(r), \quad (3)$$

where $A_k(t)$ is the slowly varying mode amplitude, ω_k and $\gamma_k(\omega_k)$ are its frequency and frequency-dependent exponential damping,[24] respectively, and $\overrightarrow{F}_k(r)$ is the normalized spatial mode distribution. Assuming the excitation source to be a localized surface plasmon mode $\overrightarrow{F}_1^{(\omega)}(\vec{r})$ at the fundamental frequency ω (for example, a far-field illumination will excite modes with most pronounced dipole moments[25]), we obtain

$$\overrightarrow{E}_{SH} = \sum_k A_k^{(2\omega)}(t)e^{-2i\omega t}e^{-\gamma_k(\omega_k)t}\overrightarrow{F}_k^{(2\omega)}(r),$$
$$\nabla\times\nabla\times\overrightarrow{E}_{SH} = -\mu_0\varepsilon(\vec{r},2\omega)\partial_{tt}\overrightarrow{E}_{SH} - \mu_0\partial_{tt}\overrightarrow{P}_{NL}. \quad (4)$$

Applying the "slowly varying amplitude" (temporal dependence) approximation, which satisfy $\nabla\times\nabla\times\overrightarrow{F}_k^{(2\omega)} = -\mu_0\varepsilon(\vec{r},2\omega)[2i\omega+\gamma_k(\omega)]^2\overrightarrow{F}_k^{(2\omega)}$, and taking the divergence

of both sides of the Eq. (4) ($\rho_{NL} = -\nabla \cdot \vec{P}_{NL}$) we obtain

$$2\varepsilon_{\text{particle}}(2\omega)\sum_k (2i\omega + \gamma_k(2\omega))\frac{dA_k^{(2\omega)}(t)}{dt}\nabla \cdot \vec{F}_k^{(2\omega)} e^{-2i\omega t} e^{-\gamma_k(2\omega)t} = -\frac{2e\varepsilon_b}{m\omega^2}\left(\frac{\omega_p^2}{2\omega^2}+1\right)(i\omega+\gamma_1(\omega))^2\left(A_1^{(\omega)}\right)^2 \times \left(\nabla \cdot \vec{F}_1^{(\omega)}\right)^2 e^{-2i\omega t} e^{-2\gamma_1(\omega)t}. \quad (5)$$

Substituting $\varepsilon_{\text{particle}}(2\omega) = \varepsilon_b[1 - (\frac{\omega_p}{2\omega})^2]$ and assuming that (i) the frequencies of interest are smaller than the plasma frequency and (ii) negligible influence of mode losses on nonexponential coefficients in Eq. (5), we obtained

$$\sum_k \frac{dA_k^{(2\omega)}(t)}{dt}\nabla \cdot \vec{F}_k^{(2\omega)} \approx i\frac{e}{m\omega}\left(A_1^{(\omega)}\right)^2\left(\nabla \cdot \vec{F}_1^{(\omega)}\right)^2 e^{(\gamma_k^{(2\omega)}-2\gamma_1^{(\omega)})t}. \quad (6)$$

Equation (6) may be reformulated in terms of surface charge densities. For this purpose we utilize the integral relation between surface charge density, which is an eigenvector of the certain Fredholm integral equation, while the localized surface plasmon frequency is defined from its eigenvalue. The corresponding boundary integral approach, defined in Ref. 26, leads to

$$\sigma(Q) = \frac{1}{2\pi}\frac{\varepsilon(\omega)-1}{\varepsilon(\omega)+1}\oint \sigma(M)\frac{\vec{r}_{MQ}\hat{n}_Q}{|\vec{r}_{MQ}|^3}dS_M, \quad (7)$$

where $\sigma(Q)$ is the surface charge density at point Q, $\varepsilon(\omega)$ is the particle's dispersive dielectric constant, $\vec{r}_{MQ}$ is the vector connecting two points on the particle boundaries—any point (M) with a point of observation (Q), $\hat{n}_Q$ is the normal to the boundary at the point Q, while the integration is performed along the particle boundary. It may be shown that $\{\sigma_k\}_{k=1}^{\infty}$ and $\{\tau_k\}_{k=1}^{\infty}$ form a biorthogonal set of functions on the particle's boundary and $\oint \tau_k(Q)\sigma_m(Q)dS_Q = \delta_{k,m}$, where $\tau_k(Q)$ is the solution of the conjugated kernel of the Fredholm equation of the second kind; τ_k has a meaning of surface dipole density.[26] Several examples of the related quantities are given in Fig. 1.

Finally, projecting Eq. (5) on the proper conjugated surface function, and taking into account that $\nabla \cdot \vec{F}$ is proportional to the surface charge density times the two-dimensional delta function at the particle's boundary, we may obtain the evolution of any particular second-harmonic resonance:

$$\frac{dA_k^{(2\omega)}(t)}{dt} = -\frac{ie}{m\omega\varepsilon_0}\left\{\frac{\oint \tau_k^{(2\omega)}(Q)\left[\sigma_1^{(\omega)}(Q)\right]^2 dS_Q}{\oint \tau_k^{(2\omega)}(Q)\sigma_k^{(2\omega)}(Q)dS_Q}\right\} \times e^{(\gamma_k^{(2\omega)}-2\gamma_1^{(\omega)})t}\frac{S}{V}\left(A_1^{(\omega)}\right)^2, \quad (8)$$

where S is the surface area of a particle and V is its volume. The maximal efficiency of the excitation will occur for the mode which maximizes the overlap integral in the curly brackets in Eq. (8). Moreover, the multiplication factor of S/V shows explicitly the proportionality to the ratio of the surface area to the particle volume. Note that the nonlinear interaction here has purely surface origin, supporting the experimental results, reported in Ref. 27.

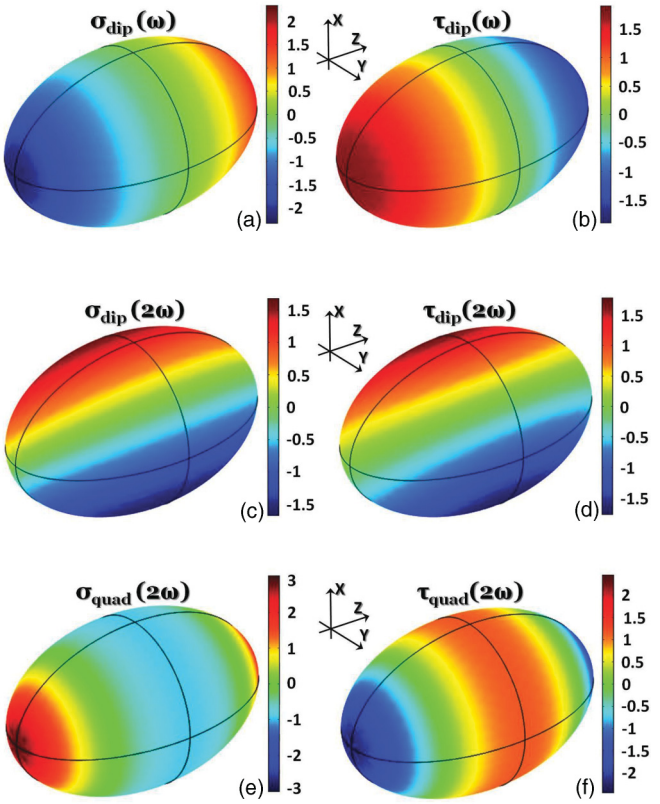

FIG. 1. (Color online) Distribution of surface charge density (left column) and the related surface dipole density (right column) for different plasmonic resonances of the spheroidal particle with the aspect ratio 1:1:1.6. (a), (b) Z-polarized dipole resonance; (c), (d) X-polarized dipole resonance; (e), (f) Z-polarized quadrupole resonance.

The conversion efficiency of the nonlinear optical processes is usually linked to the local field enhancement since nonlinear polarizabilities are proportional to a certain power of the field. Here, a similar link can be made—high surface charge/dipole density leads to high local electric fields. The "matching" integral of Eq. (8) may reach high values if these surface functions are spatially overlapped, meaning that the corresponding local fields of first and second harmonics have a significant overlap also. In particular, noncentrosymmetric particles can generate the second harmonic more efficiently. All the geometrical properties of particles are taken into account in the solution of Eq. (7) and proper matching of parameters can maximize the spatial overlap integral in Eq. (8), resulting in more efficient SHG.

III. SIMULATION RESULTS

To achieve efficient SHG into certain localized plasmon modes, a plasmonic particle should have resonances at both fundamental and second-harmonic frequencies Eq. (8). We apply our approach to the most straightforward case—single isolated spheroid particles in the free space, investigating the interplay between its different plasmonic resonances. The problem of finding localized surface plasmon resonances [Eq. (7)]

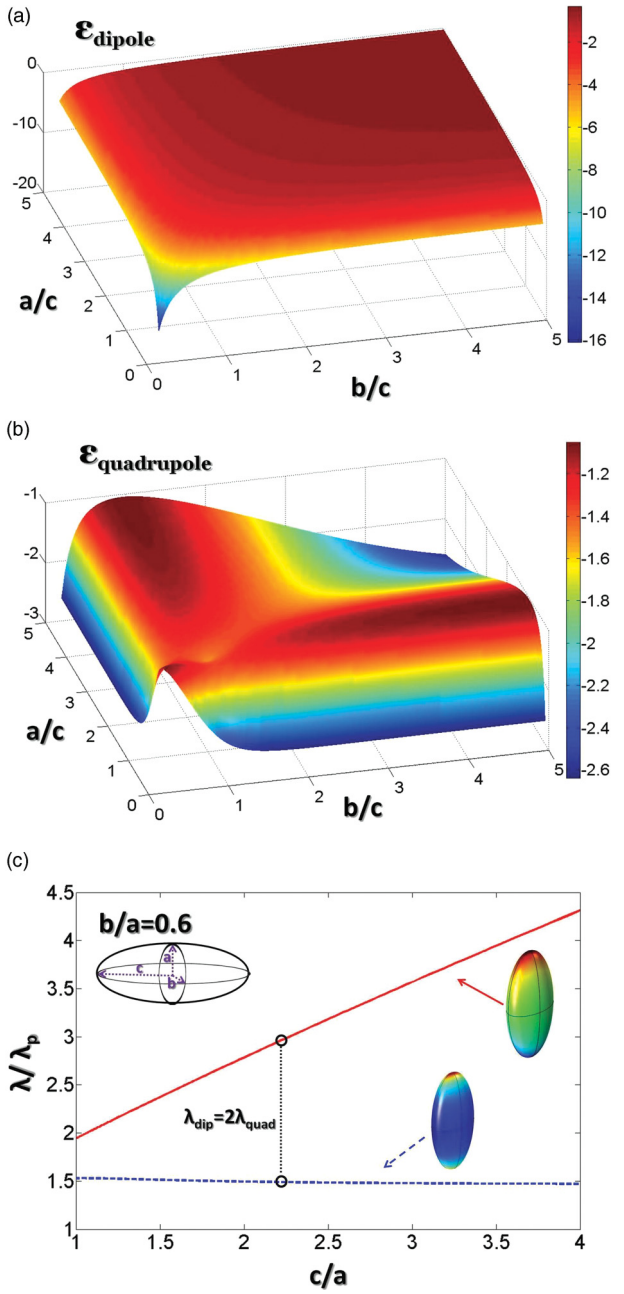

FIG. 2. (Color online) Tuning the localized surface plasmon resonances of the spheroidal particle. (a) Permittivity corresponding to Z-polarized dipole resonance as the function of particles' dimensions. (b) Permittivity corresponding to Z-polarized quadrupole resonance as a function of particles' dimensions. (c) Resonant wavelength (normalized to $\lambda_p = 2\pi c/\omega_p$, where ω_p is the plasma frequency) of dipole (red solid line) and quadrupole (blue dashed line) modes as the function of c/a parameter, while $b/a = 0.6$ is kept constant. Right insets represent surface charge densities for corresponding modes. Black vertical dotted line indicates the set of parameters for which the quadrupole and dipole modes' frequencies are matched for the SHG process. The insert in top-left part depicts the geometry of the system.

has purely geometrical formulation of determining the set of its eigenvalues α_n: $\sigma(Q) = \alpha_n \oint \sigma(M)\vec{r}_{MQ}\hat{n}_Q/|\vec{r}_{MQ}|^3 dS_M$. Then, the actual resonant frequencies can be calculated using the corresponding equation $1/(2\pi)(\varepsilon(\omega_n) - 1)/(\varepsilon(\omega_n) + 1) = \alpha_n$, defined by the actual material dispersion $\varepsilon(\omega)$. Implementing the "week form" technique in the finite-element method for solution of Eq. (7) and its conjugate, it is possible to obtain spatial distribution of surface charge and dipole densities.[28]

We consider the localized plasmon resonance at the fundamental frequency to be dipolar, since it has the highest probability to be excited with far-field excitation; however, higher-order resonances may also be considered. The surface charge density of this dipole resonance for an arbitrary spheroid is depicted in Fig. 1(a) and its square acts as a second-harmonic source. Figures 1(d) and 1(f) show the surface dipole densities for the second-harmonic dipole associated with another spheroid axis perpendicular to the fundamental dipolar mode and quadrupolar mode, respectively. Equation (8) predicts the vanishing excitation efficiency for the perpendicular second-harmonic dipole mode, since the surface integral of $\tau_k^{(2\omega)}(\sigma_1^{(\omega)})^2$ is zero. At the same time, for the quadrupole mode this overlap is nonzero, meaning that it may indeed be excited if its resonance frequency is twice that of the fundamental dipolar mode.

The problem now is to match the localized surface plasmon modes at fundamental and second-harmonic wavelengths. Two independent geometrical degrees of freedom (semiaxes of the spheroid) provide sufficient tuning abilities for this case study. Recently, it was shown that higher-order modes (quadrupoles[29] and octupoles[30]) can significantly contribute to the emission pattern of second-harmonic light. Spheroids have full analytical solutions for oblate/prolate spheroid dipole moments[31] even for higher-order modes.[32] Moreover, spheroids have a full analytical solution for the scattering problem, giving scattered field patterns and polarization-dependent cross sections.[33]

Figures 2(a) and 2(b) present the parametric plot of dipolar and quadrupolar LSPs, respectively, on the permittivity of the metal particle. The resonant frequencies were obtained using the Drude model and were plotted as the function of c/a, while $b/a = 0.6$ is kept constant [Fig. 2(c)]; the corresponding dimensions are defined in the left inset in the figure. It can be found that the resonant wavelengths of the dipolar and quadrupolar localized plasmon modes differ by factor of 2 at $c = 2.25a$ [Fig. 2(c)]. Thus, the frequency-matching conditions are satisfied for these modes. These parameters lead to the value of ~0.8 of the overlap integral [Eq. (8)]. Even higher conversion efficiencies may be achieved by additional optimizations and explorations of other geometrical shapes. Different types of resonance tuning relying on geometrical variations exist including "hybridization"[34] and "concavity"[35] techniques. Moreover, it has been recently demonstrated that several plasmonic resonances may be simultaneously tuned by employing "evolutionary" algorithms;[36] a number of other possibilities are discussed in Ref. 37. Similar approaches may be employed for additional optimization over the overlap integrals.

IV. CONCLUSION

SHG in small metal particles was investigated from first principles. In the deep-subwavelength regime the main source

of nonlinearity was shown to originate from the particles' boundaries. The conversion efficiency was shown to be proportional to the ratio of the surface area to the volume of the particle, supporting the significance of the nanoscale objects for nonlinear optical processes. Particles with high spatial symmetry will allow nonlinear conversion only between localized plasmon modes with the same symmetry properties. For example, a far-field illumination of spheroid particles will convert the energy into dark nonradiating second-harmonic modes, such as quadrupoles, however, dipole-to-dipole nonlinear coupling may be realized with particles with a lack of symmetry.

ACKNOWLEDGMENTS

The authors acknowledge support from the EPSRC program grant "Active Plasmonics." P.G. acknowledges the Royal Society for a Newton International Fellowship and Yad Hanadiv for a Rothschild Fellowship. Y.S. acknowledges funding from the Leverhulme Trust.

*Corresponding author: pavel.ginzburg@kcl.ac.uk

[1] S. A. Maier, *Plasmonics: Fundamentals and Applications* (Springer Science + Business Media, New York, 2007).
[2] S. Nie and S. R. Emory, Science **275**, 1102 (1997).
[3] M. G. Banaee and K. B. Crozier, ACS Nano **5**, 307 (2011).
[4] P. Genevet, J. Tetienne, E. Gatzogiannis, R. Blanchard, M. A. Kats, M. O. Scully, and F. Capasso, Nano Lett. **10**, 4880 (2010).
[5] M. Danckwerts and L. Novotny, Phys. Rev. Lett. **98**, 026104 (2007).
[6] A. V. Krasavin, T. P. Vo, W. Dickson, P. M. Bolger, and A. V. Zayats, Nano Lett. **11**, 2231 (2011).
[7] J. N. Anker, W. P. Hall, O. Lyandres, N. C. Shah, J. Zhao, and R. P. V. Duyne, Nat. Mater. **7**, 442 (2008).
[8] K. F. MacDonald, Z. L. Sámson, M. I. Stockman, and N. I. Zheludev, Nat. Photonics **3**, 55 (2009).
[9] Y. Pu, R. Grange, C. L. Hsieh, and D. Psaltis, Phys. Rev. Lett. **104**, 207402 (2010).
[10] W. Fan, S. Zhang, N.-C. Panoiu, A. Abdenour, S. Krishna, R. M. Osgood, K. J. Malloy, and S. R. J. Brueck, Nano Lett. **6**, 1027 (2006).
[11] C. G. Biris and N. C. Panoiu, Nanotechnology **22**, 235502 (2011).
[12] M. I. Stockman, D. J. Bergman, C. Anceau, S. Brasselet, and J. Zyss, Phys. Rev. Lett. **92**, 057402 (2004).
[13] F. X. Wang, F. J. Rodríguez, W. M. Albers, R. Ahorinta, J. E. Sipe, and M. Kauranen, Phys. Rev. B **80**, 233402 (2009).
[14] I. I. Smolyaninov, A. V. Zayats, and C. C. Davis, Phys. Rev. B **56**, 9290 (1997).
[15] R. W. Boyd, *Nonlinear Optics*, 3rd ed. (Academic Press, Amsterdam, 2008).
[16] A. Hayat and M. Orenstein, Opt. Lett. **32**, 2864 (2007).
[17] J. I. Dadap, J. Shan, and T. F. Heinz, J. Opt. Soc. Am. B **21**, 1328 (2004).
[18] O. A. Aktsipetrov, A. A. Fedyanin, E. D. Mishina, A. A. Nikulin, A. N. Rubtsov, C. W. van Hasselt, M. A. C. Devillers, and Th. Rasing, Phys. Rev. Lett. **78**, 46 (1997).
[19] R. H. Ritchie, Phys. Rev. **106**, 874 (1957).
[20] J. E. Sipe, V. C. Y. So, M. Fukui, and G. I. Stegeman, Phys. Rev. B **21**, 4389 (1980).
[21] P. Ginzburg, A. Hayat, N. Berkovitch, and M. Orenstein, Opt. Lett. **35**, 1551 (2010).
[22] M. Scalora, M. A. Vincenti, D. de Ceglia, V. Roppo, M. Centini, N. Akozbek, and M. J. Bloemer, Phys. Rev. A **82**, 043828 (2010).
[23] N. Bloembergen, R. K. Chang, S. S. Jha, and C. H. Lee, Phys. Rev. **174**, 813 (1968).
[24] P. Ginzburg and A. V. Zayats, Opt. Express **20**, 6720 (2012).
[25] I. D. Mayergoyz, Z. Zhang, and G. Miano, Phys. Rev. Lett. **98**, 147401 (2007).
[26] I. D. Mayergoyz, D. R. Fredkin, and Z. Zhang, Phys. Rev. B **72**, 155412 (2005).
[27] J. Nappa, G. Revillod, I. Russier-Antoine, E. Benichou, C. Jonin, and P. F. Brevet, Phys. Rev. B **71**, 165407 (2005).
[28] [http://www.comsol.com/].
[29] I. Russier-Antoine, E. Benichou, G. Bachelier, C. Jonin, and P.-F. Brevet, J. Phys. Chem. C **111**, 9044 (2007).
[30] J. Butet, G. Bachelier, I. Russier-Antoine, C. Jonin, E. Benichou, and P. F. Brevet, Phys. Rev. Lett. **105**, 077401 (2010).
[31] C. F. Bohren and D. R. Huffman, *Absorption and Scattering of Light by Small Particles* (Wiley-Interscience, New York, 1983).
[32] D. V. Guzatov, V. V. Klimov, and M. Yu. Pikhota, Laser Phys. **20**, 85 (2010).
[33] S. Asano and G. Yamamoto, Appl. Opt. **14**, 29 (1975).
[34] E. Prodan, C. Radloff, N. J. Halas, and P. Nordlander, Science **302**, 419 (2003).
[35] N. Berkovitch, P. Ginzburg, and M. Orenstein, Nano Lett. **10**, 1405 (2010).
[36] P. Ginzburg, N. Berkovitch, A. Nevet, I. Shor, and M. Orenstein, Nano Lett. **11**, 2329 (2011).
[37] N. Berkovitch, P. Ginzburg, and M. Orenstein, J. Phys.: Condens. Matter **24**, 073202 (2012).